Chapter 4

Photoinduced desorption of NO from Pt(111)

4.1 NO photodesorption and the Variational Wave Packet scheme

The dynamics of NO adsorbed on a Pt surface is a prototype for photodesorption problems, with many theoretical [128, 129, 10] and experimental [42, 130, 131] works, similar to the case of H_2 scattering at metal surfaces for gas surface scattering (see chapter 5). It is characterized by the femtosecond evolution for the molecule on various electronic states [10, 132] that is strongly coupled with the surface modes, in particular surface electronic excitations. Eventually, the molecule surface bond will gain energy non adiabatically and the molecule will desorb on a time scale of fractions of a picosecond, under the weak influence of electronic friction and surface phonons.

This so called DIET (Desorption Induced by Electronic Transitions) of NO from Pt (and also similar for other systems) is typically depicted as follows (see Fig.4.1 for illustration). First, the adsorbate wave packet in its ground electronic state

is promoted to an electronically excited state, either directly, or indirectly, *e.g.*, through "hot electrons". The wave packet evolves in time in the excited state (probably a metal to ligand charge transfer state in the case of NO/Pt), but is at the same time "quenched" back to the ground state, from where desorption may occur – or not. The lifetime of the excited intermediate is "ultrashort" (*i.e.*, a few femtoseconds) due to the efficient coupling of the nuclear motion to the substrate electronic excitations (*e.g.*, electron hole pairs). The surface electronic "modes" are fast and the assumption that they will induce an irreversible, dissipative dynamics is very reasonable.

Accordingly, a density matrix description should be an efficient framework for these kinds of phenomena. Indeed, the problem has been formulated within the language of open system density matrix theory, and treated with direct [133, 89, 74] as well as stochastic wave packet methods [134, 89, 90]. The challenge of the problem is twofold. First, since bonds are to be broken, a coordinate (grid) representation has to be used, leading to large Hilbert space dimensions N, in particular for multi mode models [90], making the direct approach technically intractable. Secondly, the desorption probabilities are typically very small (10^{-4}, say) and therefore stochastic wave packet methods converge very slowly when properties of the desorbates are of interest, as shown in Ref.[89].

The Variational Wave Packet method was previously applied [95], in a zero order state basis, to a bound, large, dissipative problem [88], for which three system modes and three system electronic states had to be considered, and for which the direct approach was impossible. The method gave a good performance in comparison with the equivalent MCWP calculations [88] in the computation of coherent properties. This inspired us to test the possibilities of the new method and in [96] we adapted the VWP method to the photoinduced desorption of a molecule of NO from the Pt(111) surface.

For the DIET of NO from Pt(111) we used the same one and two mode, two state models as previously [74, 90]. Since in DIET (in contrast to DIMET, "Desorption Induced by Multiple Electronic Transitions") multiple excitations of the adsorbate are not possible [74], only a single dissipative channel (namely the electronic decay)

is allowed. We assumed [74, 90] a Lindblad form for the dissipation (2.11), so the relevant dissipative Liouville-von Neumann equation reads

$$\dot{\hat{\rho}}(t) = -i\left[\hat{H}_s,\ \hat{\rho}\right] + \left(\hat{C}\hat{\rho}\hat{C}^{\dagger} - \frac{1}{2}\left[\hat{C}^{\dagger}\hat{C},\ \hat{\rho}\right]_{+}\right),$$

where $\hat{C}$ is the Lindblad operator, specifying the environment induced electronic relaxation (see below).

The system Hamiltonian $\hat{H}_s$ in Eqn.(4.1) is of the simple, decoupled two state form

$$\hat{H}_s = \hat{H}_g|g\rangle\langle g| + \hat{H}_e|e\rangle\langle e| \quad , \tag{4.1}$$

where $|g\rangle$ and $|e\rangle$ stand for the electronic ground, and the (short lived) electronic excited state, respectively. The Hamiltonians $\hat{H}_l$ $(l = g, e)$ are in the one [74] and two mode [90] models given by

$$\hat{H}_l = -\frac{1}{2}\sum_{i=1}^{F}\frac{\partial^2}{\mu_i \partial Q_i^2} + V_l(\{Q_i\}) \quad . \tag{4.2}$$

Here, in the one dimensional case $F = 1$, $Q_1 = Z$ (distance of molecular center of mass to the surface) and $\mu_1 = m_{NO}$, while in the two mode case $F = 2$, $Q_1 = Z, Q_2 = x$ (x is the NO bond length), and $\mu_2 = \frac{m_N m_O}{m_N + m_O}$.

Eqn.(4.1) is solved subject to the initial condition $\hat{\rho}(0) = |e\rangle\langle e| \otimes |0_g\rangle\langle 0_g|$, *i.e.*, an initial, singular Franck–Condon transition of the vibrational and electronic ground state wave function $|0_g\rangle$ to the electronic excited state $|e\rangle$ is assumed, as a crude model for an indirect, "hot electron" mediated excitation step [74].

Once electronically excited, the wave packet starts to move and to be electronically quenched. The quenching is controlled by the operator $\hat{C}$,

$$\hat{C} = \sqrt{\Gamma_{ge}}|g\rangle\langle e|, \tag{4.3}$$

where, $\Gamma_{ge} = 1/\tau$ is the rate for the decay of the excited state $|e\rangle$ to the ground state $|g\rangle$ (and τ is the excited state lifetime). For simplicity, Γ_{ge} is assumed to be coordinate independent. Generalization to coordinate dependent, nonexponential decay

is straightforward, and possible without much additional effort for all numerical approaches adopted below.

After a final propagation time, t_{max}, those parts of the wave packets which have reached asymptotic regions $Z > Z_d$ of the ground state potential energy surface, are counted as "desorbed", and analyzed. Of particular interest are the desorption probability, P_{des}, and the "translational temperature",

$$T_{trans} = E_{kin}/2k_b \tag{4.4}$$

of the desorbates. (E_{kin} is the kinetic energy of the neutral, desorbing NO molecules). The system has not a thermal distribution, even if it is a statistical ensemble, so the expression "translational temperature" is to be considered as kinetic energy measured in Kelvin. Since the desorption probability is small in the cases considered below, the properties associated with adsorbates are called "infrequent properties" in the following. Occasionally, we will also be interested in "frequent properties", namely the populations of the excited and ground states, and the total system energy.

The VWP results, which are obtained with n basis wave functions (excited and ground state basis), are always checked against "exact" benchmark calculations. In the one mode model, the exact reference is provided by direct density matrix propagation, based on a Newton polynomial expansion of the time evolution superoperator (see section (3.2) and references therein for the general theory and [74] for details about this system). For the two mode model a direct density matrix result is at present not available. Here, the results of Gadzuk's "jumping wave packet & incoherent, weighted averaging scheme" [41], which can be shown to be equivalent to density matrix theory for DIET models (single dissipative channel) with coordinate independent quenching rates [89] are used as benchmark. (In this case, the weighting coefficients for averaging are known analytically [89, 90]. For an extension of the economic "jumping & weighted average" approach to coordinate dependent quenching, see [90]). In the "jumping wave packet" calculations, a split propagator is used; while for any method, a discrete coordinate space representation is chosen for all occurring operators and wave functions. The action of the kinetic energy operator is evaluated locally, by using a discrete Fast Fourier Transform (FFT) algorithm (see Appendix A).

4.2 One dimensional model

In the one dimensional model, the ground state potential $V_g(Z)$ is a Morse function, and the excited state $V_e(Z)$ an image charge stabilized bound, negative ion resonance, metal to ligand charge transfer state [41]. The potential parameters are the same used in [74], and the potential curves are shown in Fig.4.1. The discrete grid used starts at $-1.4\ a_0$, and consists of $N = 512$ points spaced by $\Delta_z = 0.04\ a_0$. The desorption point, Z_d, is put at 4 a_0. The excited state lifetime is taken as $\tau = 2$ fs. The System was propagated until the desorption probabilities had reached a constant value, this corresponds to $t = t_{max} = 500$ fs. All the other computational parameters and procedures are the same as described in Ref.[74]. Let us first consider "frequent" properties associated with the decay of the excited state resonance, namely $N_e(t)$ (the population of the excited state), $N_{tot}(t) = N_g(t) + N_e(t)$ (the total norm), and $E_{tot}(t)$ (the total system energy). As shown elsewhere [89], these properties can be accurately computed with a moderate number of wave packets within the "jump & averaging" scheme, and even with the ordinary MCWP method, but, as shown in Fig.4.2, the VWP method is even more economic in the sense that a smaller number of wave functions n is required for a certain accuracy.

In Table 4.1, for the selected times $t = 2$ fs, $t = 5$ fs, $t = 20$ fs, and $t = 50$ fs the relative error for each observable $A(t)$ ($A = N_e$, N_{tot}, and E_{tot}),

$$E[A(t); n] = \frac{A_{ex}(t) - A_{\mathrm{VWP}}(t; n)}{A_{ex}(t)} \tag{4.5}$$

is given for different basis set sizes, n, of the VWP expansion (3.31). In these calculations, n was kept fixed over the entire propagation time. $A_{ex}(t)$ in Eqn.(4.5) denotes the "exact" observable, while $A_{\mathrm{VWP}}(t; n)$ is the result of a VWP calculation with n functions. Actually, the exact, frequent observables are known analytically or semianalytically in the present example [$N_e(t) = e^{-\Gamma_{ge} t}$, $N_{tot} = 1$, $E_{tot}(t) = N_e(t) \cdot E_{tot}(0) + (1 - N_e(t)) \cdot E_{tot}(\infty)$], or can be taken from direct density matrix propagation. However, we prefer to define as the exact results those obtained with the VWP method and $n = 13$, $A_{ex}(t) := A_{\mathrm{VWP}}(t; n = 13)$, in order to not spoil our analysis with (small) errors due to other numerical approximations (namely the integrator and the grid). Indeed, the VWP results for the frequent properties are

Table 4.1: Computation of "frequent" properties for the DIET of NO from Pt (see text). Shown are the relative errors as defined in Eqn.(4.5) for different numbers of basis functions, n, used in the VWP expansion. The "exact" reference is taken to be the result of the VWP ($n = 13$) calculation. The numbers in brackets (m) denote exponents (10^m).

	t [fs] $\rightarrow$	2	5	20	50
	$n = 1$	$< 1.(-8)$	$< 1.(-8)$	$< 1.(-8)$	$< 1.(-8)$
	2	$< 1.(-8)$	$< 1.(-8)$	$< 1.(-8)$	$< 1.(-8)$
N_e	3	$< 1.(-8)$	$< 1.(-8)$	$< 1.(-8)$	$< 1.(-8)$
	6	$< 1.(-8)$	$< 1.(-8)$	$< 1.(-8)$	$< 1.(-8)$
	9	$< 1.(-8)$	$< 1.(-8)$	$< 1.(-8)$	$< 1.(-8)$
	$n = 1$	6.32(-1)	9.18(-1)	1.00($\pm$0)	1.00($\pm$0)
	2	9.76(-3)	6.30(-2)	1.12(-1)	1.20(-1)
N_{tot}	3	7.06(-5)	2.94(-3)	2.29(-2)	2.29(-2)
	6	$< 1.(-8)$	3.00(-8)	5.03(-4)	5.46(-4)
	9	$< 1.(-8)$	$< 1.(-8)$	1.10(-5)	2.30(-5)
	$n = 1$	3.23(-2)	2.16(-1)	1.00($\pm$0)	1.00($\pm$0)
	2	1.42(-3)	3.98(-2)	3.74(-1)	3.75(-1)
E_{tot}	3	3.70(-7)	2.89(-3)	1.30(-1)	1.31(-1)
	6	$< 1.(-8)$	$< 1.(-8)$	6.56(-3)	7.53(-4)
	9	$< 1.(-8)$	$< 1.(-8)$	1.85(-4)	4.51(-4)

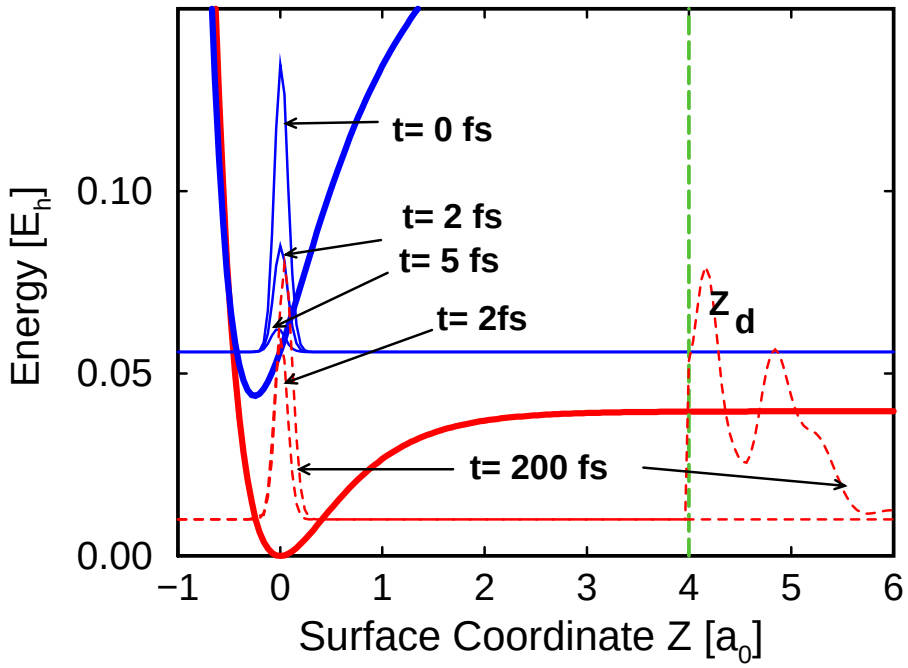

Figure 4.1: The resonance, metal to ligand charge transfer state and the ground potential energy surfaces for the NO/Pt system in the 1D model are shown as bold curves. The surface coordinate Z is the distance of the molecule's center of mass to the surface [74]. The vertical dashed line at $Z = Z_d = 4\ a_0$ is the point after which a molecule is considered as desorbed. The typical behavior of a desorption process is also shown as a series of snapshots of the diagonal elements of the density matrix, as solid curves on the excited surface and as dashed curves on the ground electronic state. The desorbed part, *i.e.*, the dashed curve after the "desorption point", is magnified 500 times.

well converged with respect to n for $n = 13$; the $n = 13$ results itself agree to within about 10^{-4} with the (semi) analytical ones. From this fact alone we anticipate that the VWP method may offer great computational savings over direct density matrix propagation schemes.

Table 4.1 shows that the "frequent" properties can be computed, to reasonable accuracy, already with much less effort. For instance, the excited state popula-

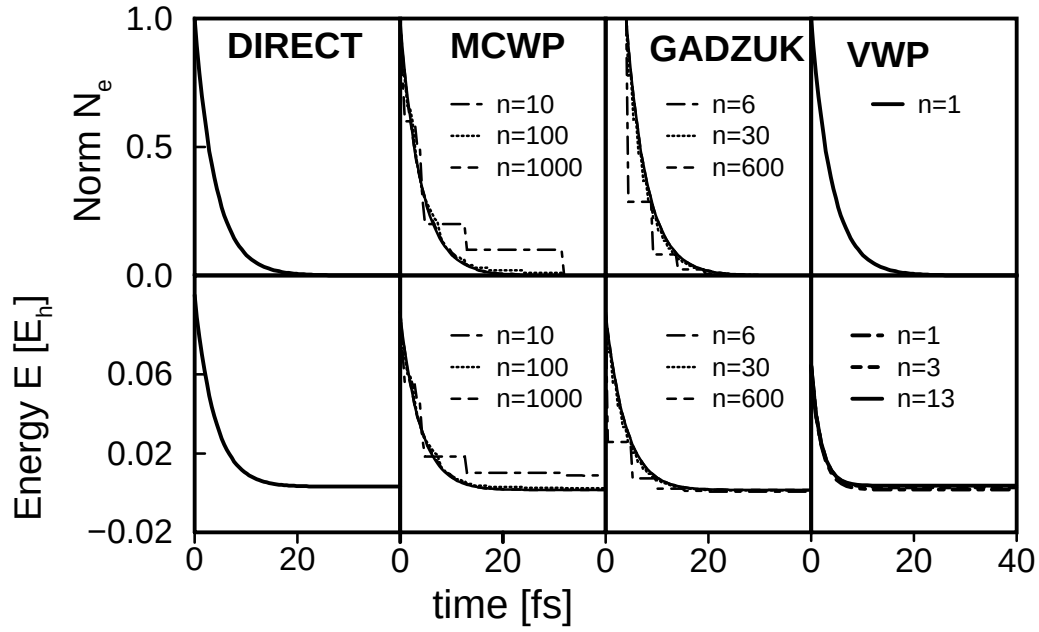

Figure 4.2: "Frequent properties" for the 1D DIET model for NO/Pt as computed with different methods are shown for different n, the number of functions used for the wave packet based methods.

tion $N_e(t)$ is *exactly* reproduced with a *single* wave function, *i.e.*, with $n = 1$ (see also Fig.4.2). This observation follows also from an analytic solution of the VWP equation (3.45) for the expansion coefficients. Namely, if only a single excited state wave function $|\psi_1\rangle$ spans the basis, the density operator $\hat{\rho}$ in Eqn.(3.31) is given by $\hat{\rho} = \rho_1|\psi_1\rangle\langle\psi_1|$; further, by using the single DIET–Lindblad operator $\hat{C}$ as defined in Eqn.(4.3), we have $\mathcal{L}_D\hat{\rho} = \Gamma_{ge}[|g\rangle\langle g| - \frac{1}{2}|e\rangle\langle e|\hat{\rho} - \frac{1}{2}\hat{\rho}|e\rangle\langle e|]$. As a consequence, the equation of motion for the coefficient $\rho_1(t)$ [Eqn.(3.45)] reads

$$\frac{\partial\rho_1(t)}{\partial t} = -\Gamma_{ge}\rho_1 \quad .$$

With $\rho_1(t) = N_e(t)$, and $\rho_1(0) = N_e(0) = 1$ it follows, that

$$N_e(t) = e^{-\Gamma_{ge}t} \quad ,$$

which is the analytical result. Any errors, relative to the analytical result, of $N_e(t)$ (and any other excited state property) obtained with the VWP method and $n = 1$,

are therefore numerical, and not due to a basis set being too small. Since in the simple DIET model used here no re-excitations are possible and no Hamiltonian couplings between $|g\rangle$ and $|e\rangle$ exist, a single wave function is sufficient to describe the excited state dynamics throughout.

Of course, for $n = 1$ the basis is (except at $t = 0$) incomplete, and total norm is not conserved; the loss of norm increases with time according to $\Delta N_{tot}(t) = 1 - e^{-\Gamma_{ge} t}$. Hence, to compute the total norm (or any observable associated not solely with the excited state), ground state basis functions $|\psi_{gu}\rangle$ must to be added. Table 4.1 shows, that one wave function in addition to the single wave function describing the excited state ($n = 2$) already suppresses (for $t = 2$ fs) the relative error from 0.632, to below 10^{-2}. This corresponds to an increase of the total norm from 0.3677 ($n = 1$), to 0.9902 ($n = 2$). When propagated to longer times, more and more wave functions are needed for a certain accuracy. To reach a total norm larger than 0.9999, say, requires $n = 3$ at $t = 2$ fs, $n = 4$ at $t = 5$ fs, and $n = 6$ at $t \geq 20$ fs (when the dissipation becomes inefficient). For all t, relative errors of the total norm (and also of the total system energy E_{tot}, for example) of 10^{-3} (and mostly much lower) are typical with $n = 6$. This is better than what was possible with the MCWP method, where in the order of $n \approx 100$ wave packet runs where needed for a comparable accuracy of the "frequent" properties [89], and also with the "jump & average" method (which required around 30 wave packets [89]), as shown in Fig.4.2.

A more stringent test of the VWP method is its performance for "infrequent" properties, *i.e.*, those associated with the desorption of neutral NO molecules. In Fig.4.3, the desorption probability $P_{des}(t)$ is given for different basis set sizes n. The number of basis functions (and the time step used by the propagator) is now automatically adjusted during the propagation, and n is to be understood as the number of functions used at $t = t_{max} = 500$ fs. The four curves shown in the figure are for $n = 7$, 9, 11, and 13, respectively. Also shown (as bullets) are the benchmark direct density matrix probabilities taken from Ref.[74], which on the scale of the figure cannot be distinguished from the most accurate VWP calculation ($n = 13$). Both "exact" curves rise after $t \approx 100$ fs from essentially zero, to the final ($t = t_{max} = 500$ fs) desorption probability of $\approx 9.5 \cdot 10^{-5}$. This small probability is not easy to capture by stochastic wave packet methods, for which even $n = 1500$

wave packets were found to not accurately reproduce the final P_{des} [89]. By contrast,

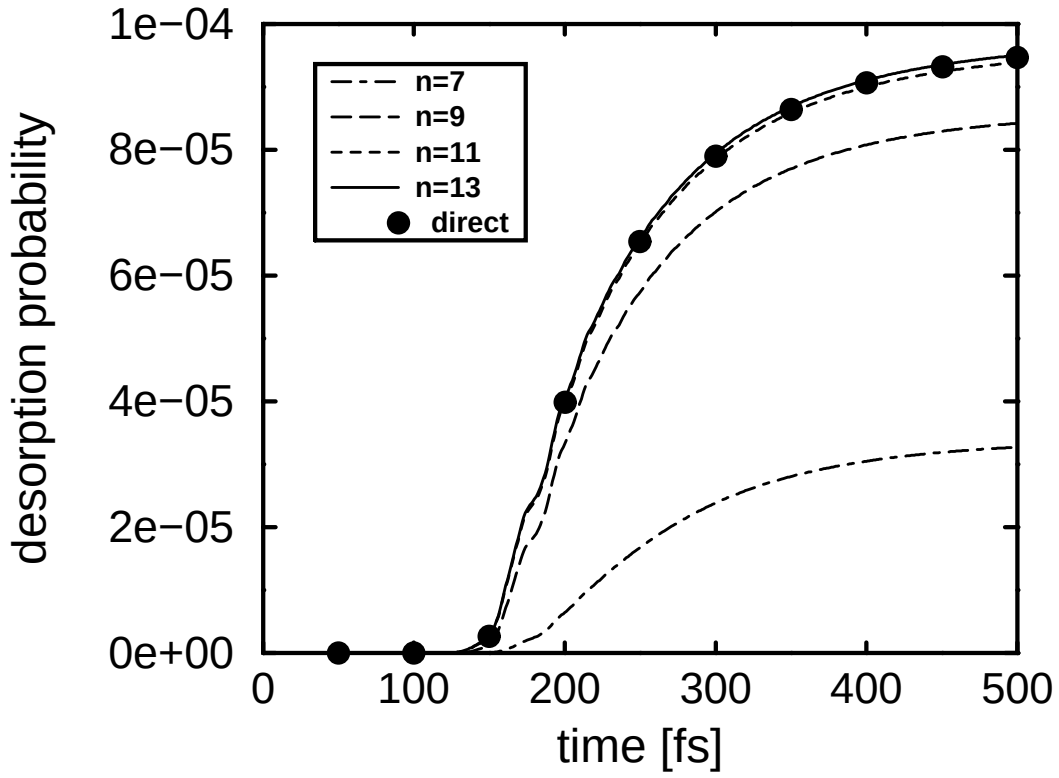

Figure 4.3: Time resolved desorption probabilities $P_{des}(t)$ for NO from Pt(111) (one mode model), as obtained with the VWP method with different basis set sizes (curves), and with the direct density matrix method [74] (bullets).

the VWP method not only converges with $n = 13$, but also with a fewer number of wave packets "reasonable" results are obtained; further, the convergence to the exact result is uniform and monotonic, rather than erratic as in the MCWP method. This happens because the method is variational and the propagation positive, so the $\rho_u(t)$ are necessarily positive and the results can only sum up together.

However, to compute "infrequent" properties, more basis functions are necessary than for the "frequent" ones.

Table 4.2: Computation of "infrequent" properties for the DIET of NO from Pt (see text). Shown are the final ($t = t_{max}$) desorption probabilities, the translational temperatures (see Eqn.(4.4)), the relative errors Eqn.(4.5) in these quantities, the loss of total norm, and the computational resources needed [the latter relative to the VWP ($n = 13$) calculation]. The "exact" reference is taken to be the direct density matrix benchmark calculation of Ref.[74], which is also included in the table.

number of wave functions n	P_{des}	rel. error in P_{des}	T_{trans}/ K	rel. error in T_{trans}	loss of total norm	relative comp. time	relative memory req.
7	3.28(-5)	6.54(-1)	491.3	4.68(-1)	2.7(-4)	0.06	0.67
9	8.42(-5)	1.11(-1)	786.8	1.48(-1)	3.4(-5)	0.15	0.72
11	9.39(-5)	8.45(-3)	907.2	1.75(-2)	4.0(-6)	0.45	0.83
13	9.48(-5)	-1.06(-3)	923.5	-1.08(-4)	5.1(-7)	1	1
direct	9.47(-5)	–	923.4	–	–	≈ 2	≈ 34

This is quantitatively analyzed in Table 4.2, where the final ($t = t_{max}$) desorption probability P_{des}, the translational temperature of the desorbates, T_{trans} (defined *via* Eqn.(4.4)), and a few other useful quantities are given, for the four VWP calculations shown in Fig.4.3, and for the direct density matrix benchmark calculation. Taking the direct density matrix result as the "exact" observable A_{ex} in Eqn.(4.5), we find moduli of the relative errors in the desorption yields between $1 \cdot 10^{-3}$ for $n = 13$, and ≈ 0.65 for $n = 7$. (The different sign of the errors for $n = 13$, suggests that this most accurate VWP propagation is in fact slightly more accurate than the numerical direct density matrix result [74].) Similar relative errors are found for the translational temperatures.

Table 4.2 also shows that the relative error in the desorption yield, say, correlates (almost linearly) with the loss of norm. Hence, errors in the infrequent properties may be brought to minimum by controlling the conservation of norm, which is a useful tool in cases where the exact answer is unknown.

Table 4.2 further tries to compare the direct density matrix propagation with the VWP method with respect to the computational effort. To make the analysis as machine independent as possible, computation time and memory requirements are given in units of the effort for the VWP ($n = 13$) calculation.

The VWP method is clearly superior to the direct, Newton polynomial approach in terms of memory needs. The ideal, theoretical ratio of the memory requirements for the VWP method with n basis vectors of length N each, and the direct density matrix approach (matrix size $N \times N$) is approximately n/N, and the "measured" ratios found in Table 4.2 are of the expected order of magnitude. Since the VWP approach is a coupled wave function method, the storage requirement is, however, less favorable than for the MCWP method, for example, which has an ideal ratio of n/N , and moreover is trivial to parallelize.

With respect to the computation time needed for a VWP(n) calculation, we find in good approximation a numerical scaling proportional to n^2. Up to $n = 13$, for the present example, the VWP method is also faster than the direct method. However, this statement is somewhat ambiguous since vastly different algorithms were used for both methods. The "waste" of memory by direct methods, and the convergence

Table 4.3: Eigenvalues of the (ground state block of the) density matrix (right column), compared to the ground state expansion coefficients of the variational wave packet method, for different n, at $t = t_{max}$. [The expansion coefficient of the (single) excited state wave function is zero.]

	$n = 7$	$n = 9$	$n = 11$	$n = 13$	density matrix
1	.880225719	.880226017	.880226026	.880226018	.880226024
2	.096868957	.096874711	.096875082	.096875098	.096875100
3	.017190538	.017201899	.017202689	.017202743	.017202747
4	.004005631	.004020574	.004021669	.004021746	.004021755
5	.001106745	.001126925	.001128210	.001128300	.001128309
6	.000327787	.000356115	.000357609	.000357715	.000357725
7		.000119952	.000121829	.000121948	.000121958
8		.000040422	.000042752	.000042890	.000042901
9			.000015012	.000015183	.000015195
10			.000005110	.000005363	.000005378
11				.000001879	.000001901
12				.000000610	.000000650
13					.000000246
14					.000000083
15					.000000022
16					.000000013

properties of the VWP method can be demonstrated by diagonalizing the 512×512 ground state block of the density matrix. In doing so, we find that for $t = t_{max}$ only 16 eigenvalues are larger than 10^{-8} (see Table 4.3). This implies that in its diagonal form most of the density matrix elements are zero, and are propagated and stored without carrying any useful information. It implies further, that in order to obtain results with eight significant digits, $n = 17$ has to be chosen, while with $n = 13$ six significant digits are obtained.

Table 4.3 also gives the n eigenvalues (*i.e.*, the expansion coefficients ρ_u) of the density matrix in the VWP representation, for the four different calculations reported in Table 4.2. Inspection of the Table 4.3 shows that the VWP method tries to represent the "exact" (diagonal) density matrix with a minimum number of basis functions in an optimal fashion (as should be expected, since $\hat{\rho}$ is represented in the natural orbital base). The "frequent" properties considered above are determined by the largest eigenvalues, which are well represented already with a few basis functions. For the computation of the "infrequent" properties, however, smaller (but not the smallest) eigenvalues turn out to be important, and larger n are required to accurately represent those. The reason for this is simply that the less populated functions derive from the initial function (the only one on the excited surface), at later time. Since this one has moved closer towards the equilibrium position of the excited surface, the new functions are created deeper in the repulsive part of the ground state potential and have thus a better chance to desorb.

4.3 Two dimensional model

In the two mode model, additional to the molecule surface distance Z, the NO vibrational coordinate is included. The 2D potential energy surfaces for the neutral ground state and the excited state negative ion resonance are taken from Ref.[135], with two modifications [90]: (i) The parameter for the NO equilibrium distance $x_{0,e}$ in the excited state is reduced from 2.377 a_0 to 2.193 a_0, because the vibrational excitation generated by the former value is incompatible with the experimental results; (ii) the energy difference between V_e and V_g at the Franck–Condon point

is reduced to 1.5 eV, to account for the experimentally estimated excitation energy [136]. Compared to Ref.[90], an enlarged grid along x with $N_x = 64$ (grid spacing $\Delta_x = 0.03$ a_0), and a finer grid along Z with up to $N_Z = 1024$ (grid spacing $\Delta_Z = 0.02$ a_0) is used, to describe better the kinetic energy distribution. The lifetime chosen is $\tau = 10$ fs, which produces somewhat larger (and numerically easier accessible) desorption probabilities than in the one mode example. Thus showing that the increased dimensionality effectively changes the behavior of the dynamics of the system, allowing for a much longer lifetime for the excited electronic state. The total propagation time is $t_{max} = 700$ fs.

This time, no direct density matrix calculation is possible, because the grid consists of $N = 65536$ points, and therefore $4 \cdot 2^{34}$ elements had to be stored for a single, two state density matrix. A benchmark, however, can be provided by Gadzuk's "jumping wave packet" algorithm [41] for the special DIET model at hand. The "jumping wave packet" calculation was performed on the full 1024×64 grid. Only quenching $\sqrt{\Gamma_{ge}}|g\rangle\langle e|$ Lindblad operators were used (see Eqn.4.3), so the evolution is dissipative only for the first ≈ 80 fs, because later on there is no more appreciable population on the excited surface. The functions $|\psi_u(t)\rangle$ being coupled by the VWP equations of motion (3.49) only if the dynamics is dissipative, the heavy part of the propagation can be consequently described on a much smaller grid, *i.e.*, with less than 256 points in the Z direction. In fact the grid was adapted during the propagation by enlarging it when one of the functions $|\psi_u(t)\rangle$ reaches the edge of it. For the remaining nondissipative evolution, the wave functions were propagated independently and the observables computed using relation 3.31. For the "frequent" properties the results are completely equivalent to the one dimensional case, *e.g.*, the properties on the excited surface can be computed with only one function. Considering "infrequent" properties, with the "jumping wave packet" approach a final desorption probability of $2.45 \cdot 10^{-2}$, and a translational temperature of $T_{trans} = 1840$ K is obtained. With the VWP method, two calculations were performed. In a first calculation, $n = 13$ basis functions were used, leading to $P_{des} = 1.83 \cdot 10^{-2}$, and $T_{trans} = 1610$ K. In a second calculation, $n = 34$ was chosen, giving $P_{des} = 2.32 \cdot 10^{-2}$ and $T_{trans} = 1860$ K, which is (considering the differences in the numerical realization) in good agreement with the benchmark result. Again, based on the loss of total norm, an internal accuracy check for the VWP method

can be made. The loss of norm is $\approx 10^{-3}$ for $n = 13$, and $\approx 10^{-4}$ for $n = 34$, and the estimated relative errors are one order of magnitude larger. The two calculations took around 2 and 10 days, respectively, on an Origin 2000 SGI workstation.

In Fig.4.4, the dynamics is approximately depicted. For the VWP scheme, the arrow on the excited potential energy surface represents the first $|\psi_0(t)\rangle$, after its Frank–Condon excitation. During its evolution on the higher energy surface, the wave packet generates the other functions $|\psi_1(t)\rangle$, $|\psi_2(t)\rangle$ ... on the ground surface. As it was for the one dimensional model, the later the wave functions are generated the further they will be away from the equilibrium position, because $|\psi_0(t)\rangle$ moves towards the excited surface minimum, that is located at a smaller Z and a larger r, compared to the ground surface. The number of functions needed to converge the two dimensional calculations are larger than the one needed for the one dimensional case. This is due to the fact that the increased dimensionality generates a more dense states distribution, as is also known in many dimensional eigenstate calculations. The expansion (3.31) necessary to approximate $\hat{\rho}(t)$ is accordingly "longer", the decay of the $\rho_u(t)$ with the number u being less strong. These two calculations on the two dimensional system were performed to show that the method can effectively be used for systems too large to be handled with direct integration (see chapter 3) and where the many dimensional large grids imposes a careful design of integration algorithms, *e.g.*, the use adaptative grids.

Because of its simple structure, this DIET model can be handled very efficiently with the Gadzuk method and its generalizations [90], thus allowing to produce benchmark calculations to determine the numerical properties of the method, and check its error estimators.

The calculations done by Gerdts et al. [95] together with the calculations shown in this chapter prove that the VWP method is a general and reliable tool to treat large scale problems. The calculations in Ref.[95] refer to a large three dimensional bound model system intended to reproduce the dissipative dynamics of the S_1/S_2 states of pyrazine, while our work extended the modeling to unbound dissociative dissipative systems. This point is discussed more in detail in the "Conclusions and outlook", chapter 6, this section having to be understood more as a methodological

necessary step towards the treatment of larger systems than as a self contained physical simulation.

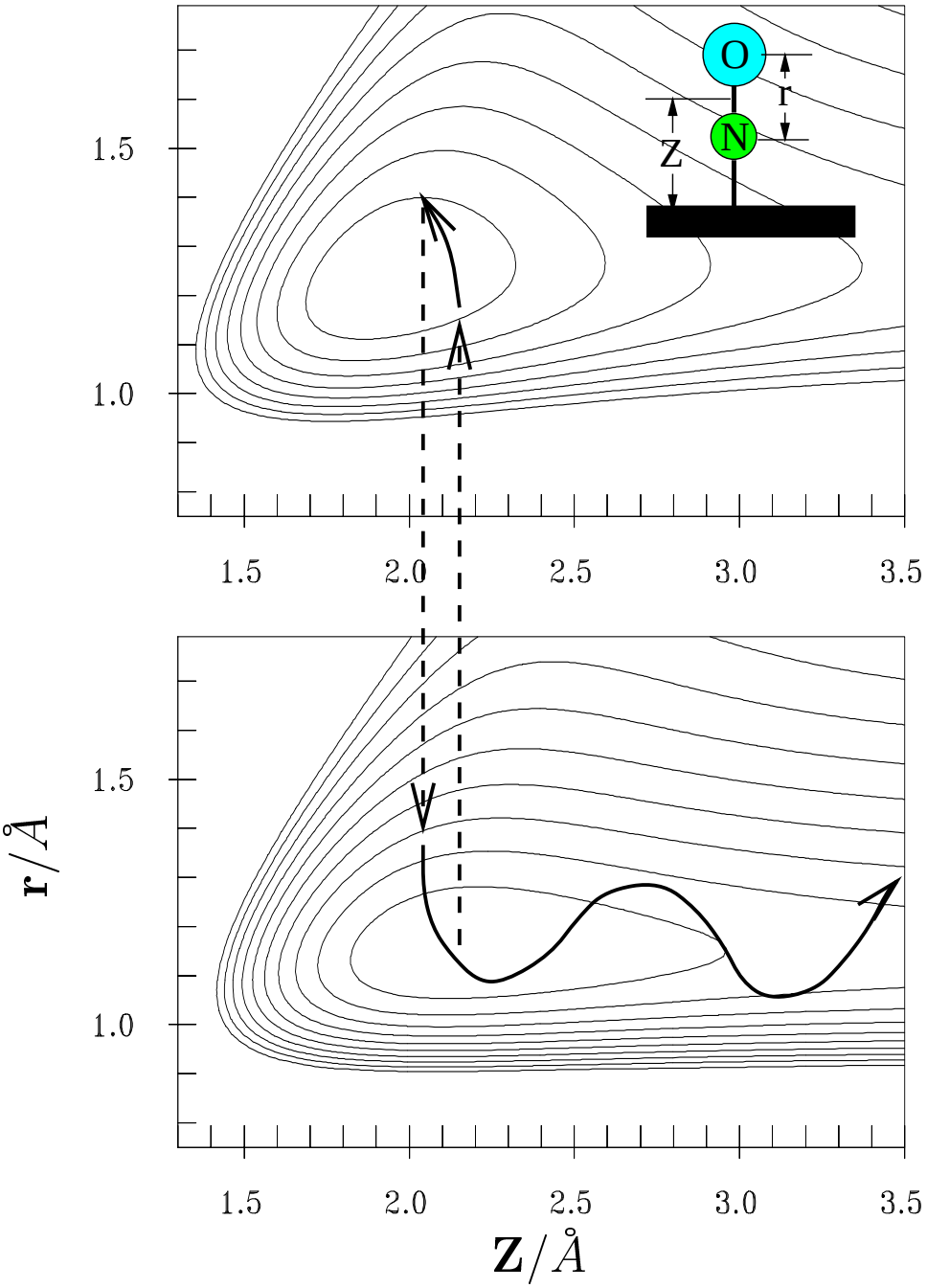

Figure 4.4: Contour plot of the model potential energy surfaces, $V(r, Z)$. The insert shows the meaning of the coordinates r and Z, respectively. The top panel shows the resonance, metal to ligand charge transfer state, while the bottom panel shows the ground state. The potential is adapted from Ref.[135] modifying it as indicated in the text. The contour spacing is 0.6 eV. The bold curves indicates the nuclear motion during the dynamical event, while the dashed lines show the electronic transitions between the two surfaces [after [90]].